Development of the radio frequency quadrupole proton linac for ESS-Bilbao

J.L. Muñoz,* I.Bustinduy, D. de Cos,† I. Rueda, and A. Ortega
ESS-Bilbao , Ugaldeguren III, Polígono A-7B, 48170, Zamudio, Spain
(Dated: January 30, 2018)

The Radio Frequency Quadrupole (RFQ) linear accelerator for ESS-Bilbao is described. This device will complete ESS-Bilbao injection chain after the ion source and the LEBT. The design was finished in 2015 and machining of the accelerator cavity started in 2016. The RFQ is a 4-vane structure, aimed to accelerate protons from 45 keV to 3.0 MeV and operating at 352.2 MHz in pulsed mode with a duty cycle up to 10%. Total length is about 3.1 m divided in 4 segments. Each segment is itself assembled from four components, named vanes, by using polymeric vacuum gaskets with no brazing among them. Notable aspects of the design are the constant mean aperture R_0, vane radius ρ and thus ρ/R_0 ratio and also uniform intervane voltage. Novel procedures for the design of the modulation and integrated beam dynamics and electromagnetic design have been developed for this task. In this paper, the complete design procedure and its results are presented, including beam dynamics, RF cavity design, field flatness and frequency tuning, cooling and thermo-mechanical design.

I. INTRODUCTION

ESS-Bilbao[1] is the institution designated to supply Spanish in-kind contribution to European Spallation Source ERIC (ESS[2]). Contributions involve the accelerator (complete MEBT, Medium Energy Beam Transport, section), the target and part of the neutron instruments. In addition to the in-kind contribution to ESS local projects are also under development. The main goals of the local facilities are to test components for ESS project and to become the first stages of a future accelerator. The ESS-Bilbao local activities are related to the setting-up of a proton injector consisting on an ECR (Electro Cyclotron Resonance) ion source and a LEBT (Low Energy Beam Transport) system, already in operation[3]. The injector will be completed with the RFQ linac presented in this communication.

The ESS-Bilbao RFQ design was carried out by a local team taking the designs for ISIS-FETS[4] and Linac4[5] RFQs as references, but choosing completely non-standard design options (round lobes, constant mean aperture and vane radius, cooling channels design or no-brazing assembly, among others). After a review by a panel of experts in 2013, the RFQ underwent a major revision that resulted in the present design. The complete design process including the modifications has been collected in a Technical Design Report (TDR)[6]. This paper discusses the different approaches and the design route chosen and the corresponding tools that have been used. The conclusions can be useful to other groups attempting to design an RFQ linac.

The non-conventional approach to the design of the modulation and the resonant cavity needed the design of home-made computer tools or to adapt existing ones. The software used for each design step will be described in the corresponding section. The RFQ is currently under fabrication, and first tests are expected to start during 2017.

A. RFQ Characteristics

Design choices on the ESS-Bilbao RFQ design are a consequence of the nature of the project. The aim was not to replicate conventional designs but to maximize R&D aspects in order to train the local team in accelerator components design, fabrication and operation.

The RFQ is divided in four segments of around 800 mm in length. Each segment is itself an assembly of four components, two major vanes and two minor vanes, as described in Fig. 1. The vanes are assembled by means of polymeric vacuum gaskets (3D O-rings) with no brazing or welding. This strategy was adapted from the ISIS-FETS RFQ[4], and was also proposed for other projects[7]. The vacuum ports in the upper and lower major vanes are also taken from FETS RFQ. However, the cooling scheme is different from this RFQ, as we use drilled channels for the vacuum grid and along the vane tips instead of the cooling-pockets.

As an additional difference to FETS RFQ, we plan to use the cooling water temperature to tune the RFQ operation, instead of using movable plunger tuners. Nonetheless, the use of movable plunger tuners is kept as an open alternative to our RFQ operation. The first segment (shown in this report) has only cooling channels along the vane tips (not in the structure body). This was decided by mechanical and fabrication criteria, and tuning was designed with this characteristic in mind. This means that the frequency control by the cooling water temperature will also be non-conventional for segment 1. After we have verified that the fabrication has being done without incidences, the body channels will be reconsidered for segments 2-4.

The RFQ is designed to accelerate protons from 45 keV

* jlmunoz@essbilbao.org
† Now at Departamento de Física Aplicada II, Facultad de Farmacia, Universidad del País Vasco, Paseo de la Universidad 7, 01006 Vitoria-Gasteiz, Spain

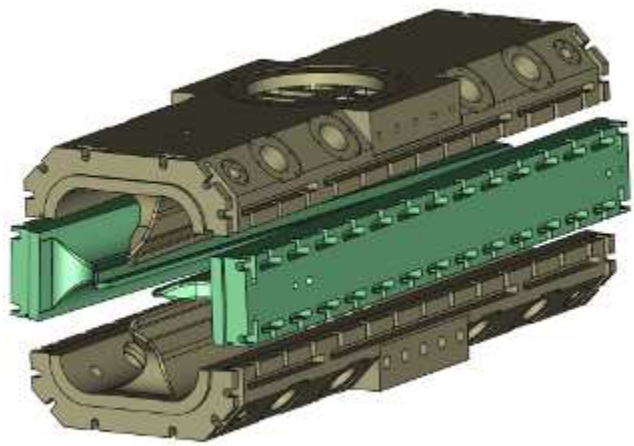

FIG. 1. Exploded view of first segment of the RFQ, showing the so-called major and minor vanes.

TABLE I. ESS-Bilbao RFQ Main Characteristics.

	ESS-Bilbao RFQ 2015 design
Type	4 vane
Particle	Protons
RF frequency	352.2 MHz
Intervane Voltage	85 kV (uniform)
Energy	45 keV $\longrightarrow$ 3.0 MeV
Design current	60 mA
Input emittance (rms norm)	0.25 π mm mrad
Duty cycle	Up to 10%
Kilpatrick factor	1.85
Number of cells	273
R_0	3.44 mm
ρ/R_0	0.85
Input/Output matcher	16.674 mm / 14 mm
Total length	3.12 m (3.66 λ)
Number of segments	4 (about 800 mm each)
Method of assembly	Polymeric vacuum gaskets
Plunger tuner ports	16 per segment

to 3.0 MeV. It is a pulsed machine, operating at 352.2 MHz with an expected duty cycle in operation of 4% (designed up to 10%). Notable aspects of the design are the constant mean aperture R_0, vane radius ρ and thus ρ/R_0 ratio. Intervane voltage is also designed as uniform, with a value of 85 kV. Main characteristics of the RFQ can be found in Table I.

In each segment there are 16 tuner ports (⌀37 mm) that can be used for static plunger tuners. The power coupler flange also fits in these ports, so that they can be inserted in any position. Additionally, 8 ⌀16 mm ports are built in order to be used for pick-ups or other sensors needed at any moment. Vacuum grid ports are designed for standard ⌀210 mm flanges. All ports are machined in the major vanes.

II. MODULATION AND BEAM DYNAMICS

A. Modulation design

The ESS-Bilbao RFQ modulation is the result of an optimization process. The modulation is designed for an intervane voltage of 85 kV, uniform throughout the entire length. Vane radius (ρ) is also constant, so to obtain a uniform local frequency and field flatness the mean aperture R_0 should also be constant. Modulation shape is based on a 2-term expansion of the intervane voltage[8] and has been designed using a modified version of RFQSIM code[9].

The aim of the modulation design was to obtain an RFQ shorted than $4\lambda = 3.4$ m to simplify tuning operations. Also, copper blocks 800 mm long were already available, so an additional target was to fit the total length of the RFQ in four segments, instead of five, reducing inter segments joints and the risks associated. A final length limit of 3.1 m was selected.

Another figure of merit target for optimization was the Kilpatrick factor (ratio of designed maximum electric field value with respect to the theoretical maximum for copper at the operating frequency), that was chosen to be below 1.85.

1. *Modulation optimization process*

The optimization procedure takes as input a set of modulation parameters, that is processed by the modified (2-term) version of RFQSIM code. Why we need the limit to two terms of the expansion is described in another section. Modulations are, in a first stage, created and analyzed using

The input parameters defining a modulation are (the standard parameter naming convention is used[10]): synchronous phases and particle energy at the end of each section (Shaper ($\phi_{\rm sh}$, $W_{\rm sh}$), Gentle Buncher ($\phi_{\rm gb}$, $W_{\rm gb}$) and Accelerator ($\phi_{\rm f}$, $W_{\rm f}$)), clear aperture ($a_{\rm gb}$) and modulation ($m_{\rm gb}$)) parameters, and input and output matcher sections radius.

In order to design a modulation with this short length the range of parameters during optimization was oriented towards this target, with preference over other goals such as maximizing the transmission or maintaining a conservative Kilpatrick factor. In this sense, we concentrated the parameter space search on areas with lower clear aperture $a_{\rm gb}$ and energy $W_{\rm gb}$, and less negative synchronous phase $\phi_{\rm gb}$ (all referred to the end of the Gentle Buncher). Particle tracking results obtained with RFQSIM presented transmissions below 90 % for modulations found in this region of the parameter space. However, later simulations with other codes presented much better results. This strategy also produced higher surface fields, with a peak at the end of the Shaper typically above 1.8 times the Kilpatrick limit.

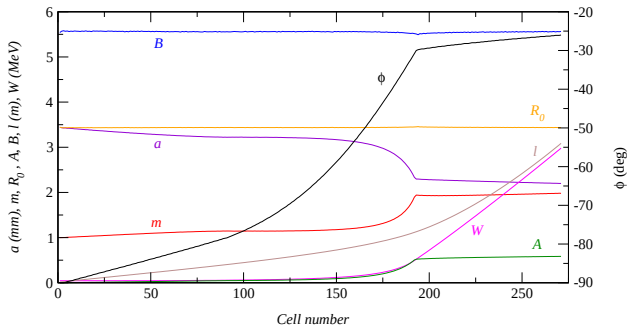

FIG. 2. Evolution of several modulation parameters as a function of the cell number.

Also, a progressive reduction of the aperture in the Acceleration section was implemented in order to shorten the modulation. RFQSIM originally built the 2-term based Acceleration section using a constant aperture and modulation factor, following the rules proposed by Kapchinskiy-Tepliakov[8]. This produces slowly decaying fields along z, due to the increased cell length. We modified the part of RFQSIM that creates the 2-term modulation to incorporate custom aperture reduction strategies in the Acceleration section, as well as the ability to set a goal total length for the modulation.

The evolution of the main parameters as a function of cell number is shown in Fig. 2, while the final modulation shape and the corresponding accelerating field are shown in Fig. 3.

Concerning the high energy end of the modulation, it has been designed with the aim of optimizing the transmission through the designed MEBT and DTL. After the last regular cell of the accelerator section, a transition cell is included so both X and Y vanes end with the same aperture. A circular output matcher ends the modulation. The transition cell has a length of 17 mm and the output matcher has a radius of 14 mm. The last cells are shown in Fig. 4.

B. Surface field calculations

Although RFQ design software packages provide a calculation of Kilpatrick factor (surface electric field) we preferred to make this calculations in an external finite element software in order to gain control and accuracy over the process. From the modulation description obtained from RFQSIM we got the modulation amplitude at the beginning and ending of each cell (of length $\beta\lambda/2$). The shape of the modulation is built cell by cell by performing the 2-term interpolation in a Matlab script, obtaining the modulation curves $V_x(z)$ and $V_y(z)$ for horizontal and vertical vanes, respectively. The cell 3D geometry vane region is then built as a parametric surface for each vane in COMSOL Multiphysics FEM software. For example, the geometry of the profile of an horizontal vane cell between z coordinates z_0 and z_1 is defined as a parametric surface dependent on parameters $u \in [0, 1]$ and $v \in [-\pi/2, \pi/2]$ as defined in Eq. 1. Vertical vanes are defined in a similar way.

$$\begin{cases} x = V_x(z(u)) + \rho(1 - sin(v)) \\ y = \rho\, sin(v) \\ z = z_0 + u(z_1 - z0) \end{cases} \tag{1}$$

The surface field is computed running an electrostatics simulation. To avoid border effects in the simulations, the model is built for three consecutive cells, considering the results only for the cell in the middle. For a given modulation, the process is fully automated using Matlab/COMSOL scripts. The results are the curve $E_{s,max}(z)$, where for each cell starting at coordinate z the maximum value of surface field computed in the cell surface is plot, and also the maximum value of the curve, that is taken as the figure of merit characterizing the particular modulation. Using this approach we managed to scan a huge and fine set of parameter ranges in an automatic, brute-force approach. An example of such electrostatics model is shown in Fig. 5.

The obtained results for the selected modulation is shown in Fig. 6. The peak at around $z = 0.5$ m is caused by the transition between Shaper and Gentle Buncher sections, while the gradual increase from $z = 1.3$ m is a consequence of designing for higher accelerating fields in order to reduce modulation length.

Surface field calculations have also been used to determine the shape and position of gaps between the segments. The modulation design is a continuous function from the beginning of the input matcher to the end of the output matcher, but in reality the segmentation of the RFQ structure means that the modulation has to be cut at certain z coordinates. In order to reduce the perturbation that these cuts cause on the electric field, extensive simulation studies were made[6]. In these studies the position of the end-beginning of segments were considered between the cell-end position and the Lloyd position [11]. In the first case the longitudinal accelerating field is zero for all particles in the gap, but not the transverse components. In the second case, the field vanishes when the bunch center crosses the gap. Also, the shape of the vane tips was studied, finally selecting an elliptical shape instead of a circular one. These studies included surface field calculation and also beam dynamics simulations. The overall best results, considering figures of merit and segment mechanical length conclusion was to use gaps of 200 µm long placed at the end-cell position; the end pf the vanes are rounded with an elliptical shape having long and short semi-axes of 2 mm and 0.75 mm respectively (see Fig. 7).

C. Beam dynamics results

From the 2-term interpolation of the modulation points the full-vane 3D geometry was built in COMSOL Mul-

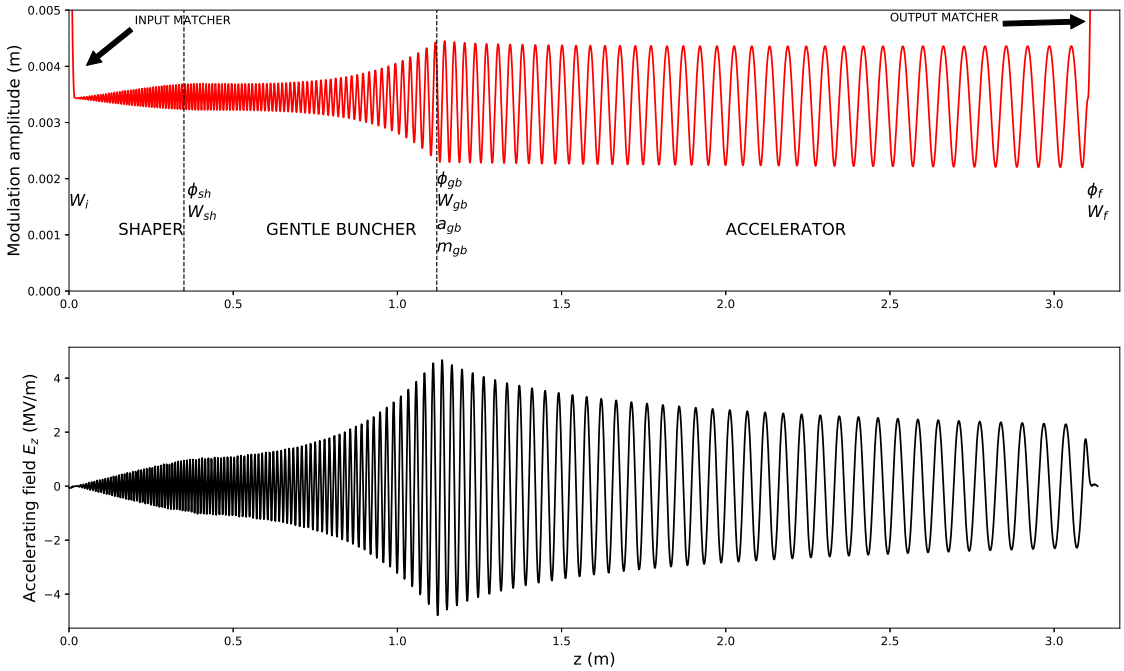

FIG. 3. Modulation amplitude and accelerating field for ESS-Bilbao RFQ.

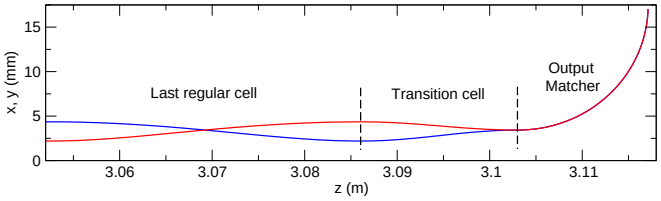

FIG. 4. Characteristics of the last cells of the RFQ.

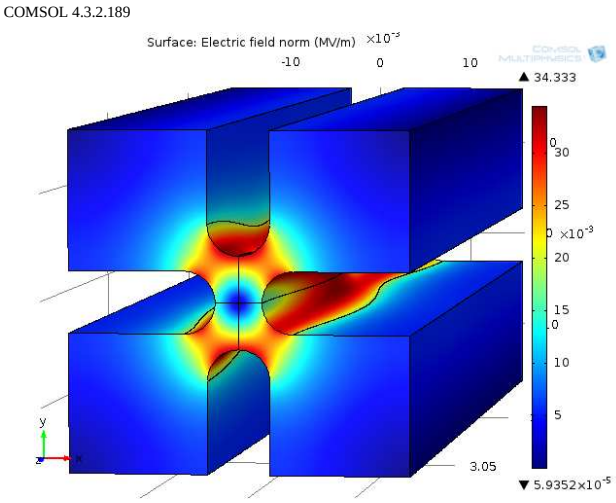

FIG. 5. Surface electric field in an electrostatics model of three cells computed to extract the maximum surface field per cell. Only the vane region is considered for the calculation.

tiphysics software. Electrostatic simulations were run and the electric field result exported for particle tracking analysis using GPT[12] particle tracer code. Several optimization runs were made, exploring different regions of the parameter space until a the final modulation was obtained. Results were then cross-checked using different codes (Toutatis[13], PARMTEQ / RFQGen). Some characteristics of the modulation can also be found in Table I.

Beam dynamics simulations have been performed under the same basic conditions in all the codes used (45 kV input beam energy, 60 mA current intensity and 0.25 π mm mrad of transverse emittance). The C-S (Courant-Snyder[10]) of the input beam varied slightly from code to code, depending on the optimal match calculated in each case, with alphas typically a little above 1, and betas about 0.03 m/rad.

We have performed beam tracking simulations with four different codes: GPT + COMSOL, RFQSIM, TOUTATIS and RFQGen (an improved fork of PARMTEQ). The implementation of our design in RFQGen is not completely accurate, since this code did not include an option to import a cell-by-cell description of the modulation at the time. So in consequence, the current RFQGen results

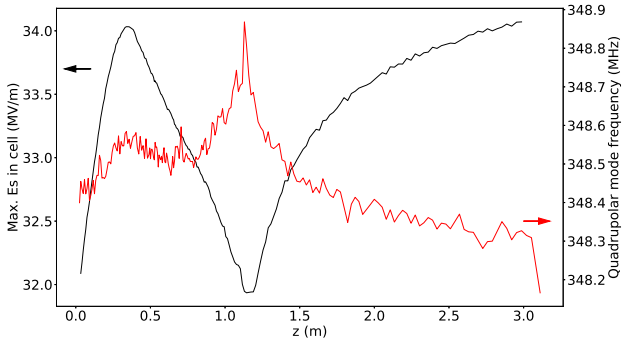

FIG. 6. Surface maximum electric field per cell (left) and local frequency (right) as a function of cell starting coordinate z. Frequency is calculated in a slice of RFQ with one cell length and no tuners.

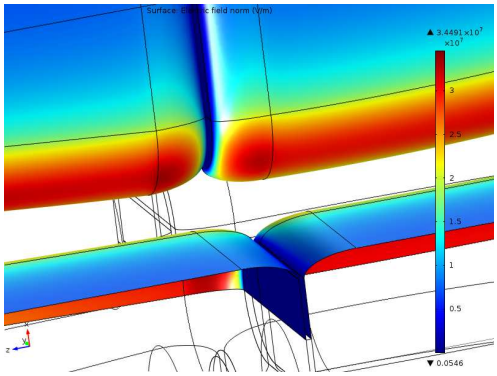

FIG. 7. Electric field in the surface of vane tips around a gap between segments. The shape of the end of the vanes is elliptical.

must be considered as approximate.

Table II presents the main results of the particle tracking simulations. The accelerated ($\sim$ 3 MeV) beam transmissions of TOUTATIS, GPT + COMSOL and RFQGen are almost identical ($\sim$ 94 %). The emittance results are very positive, with virtually null increase of the transverse emittance, and a value of 0.12–0.13 deg MeV for the longitudinal emittance.The

TABLE II. Simulation results at the output of the RFQ for the four methods used. The figures of merit are: full transmission (%), accelerated transmission (%), transverse normalized rms emittance (π mm mrad) calculated as the average between the horizontal and the vertical values, longitudinal rms emittance (π deg MeV) and maximum surface electric field (MV/m).

Simulation method	T_{all}	T_{good}	ϵ_t	ϵ_z	E_s
RFQSIM	90.7	86.8	0.243	0.120	30.4
TOUTATIS	94.6	93.6	0.266	0.131	33.4
GPT + COMSOL	95.2	94.1	0.264	—	34.1
PARMTEQ/RFQGen	96.2	94.1	0.241	0.125	33.7

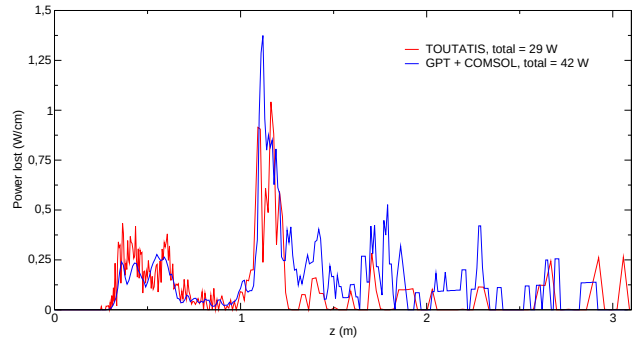

FIG. 8. Beam power loss per centimeter of RFQ length, simulated with two different methods.

surface fields, while not identical (they are calculated by different approaches), lie within 1.81–1.85 times the Kilpatrick limit (18.47 MV m^{-1} for 352.2 MHz).

RFQSIM, however, gives a poorer transmission that the other three codes, which is mainly due to a predicted transverse loss of almost 10 % of the beam. We have investigated this effect, but no definitive conclusions have been drawn. In any case, we are confident that the other three codes represent the actual transmission of the RFQ more accurately, given that TOUTATIS and RFQGen (PARMTEQ) are the most widely used codes in the field of RFQ beam dynamic and that the field maps provided by COMSOL comes from a finite element simulation with accurate representation of 3D vane geometry, and the tracking is performed with GPT, a code extensively used beam dynamics simulations of other accelerator elements.

Fig. 8 shows the transverse losses (due to particles impacting with the vanes) along the RFQ, by depicting the beam power lost per centimeter of length. The curves are very similar in the Shaper and Gentle Buncher regions (first 1.2 m), with slightly higher power loss predicted by GPT + COMSOL in the Acceleration section. The total power lost (integral of the curves) remains within reasonable values in both cases, since most of the lost particles impact the vanes with energies in the hundreds of keV.

In summary, the results presented above prove the validity of the proposed vane modulation in terms of beam dynamics, as tested with different particle tracking and field map calculating methods. Although some of the new design constraints (especially the $\sim$20 % length reduction) were initially expected to reflect negatively on the beam transport performance, this is only apparent in the RFQSIM results, with the other three codes presenting transmissions of $\sim$94 %.

D. Local frequency profile

The geometry of the vane modulation is perturbation to the ideal quadrupole resonator. This perturbation depends on the modulation amplitude and on its particular shape. Considering a modulation cell that is located

between z_i and z_{i+1}, the local frequency $f_q(z_i)$ is the frequency of the resonator built from a slice of RFQ volume between z_i and z_{i+1}, with perpendicular magnetic field boundary conditions at both ends and perfect electric boundary condition at the rest of the surfaces. This local frequency is a key characteristic for the the adequate tuning of the RFQ cavity and it is an input for the mathematical transmission line model described in section IV B.

This frequency profile should be as flat as possible because voltage profile in the real cavity will be dependent on this perturbation[10]. For the first design of ESS-Bilbao RFQ a sinusoidal vane profile was used, resulting in a very perturbed frequency profile[6]. For the final design a 2-term modulation shape (meaning that the geometry mimics the profile of an expansion of voltage truncated to two terms) was used, resulting in the rather flat profile shown in Fig. 6. Deviation of local frequency around the 2D ideal design frequency is of the order of 0.1 MHz, while with a sinusoidal shape it was of several MHz (see the TDR[6] for details).

III. CAVITY DESIGN

A. Cavity cross-section design

The cross section of the cavity is based on the circular lobe approach used by ISIS-FETS[4], but with modified straight vane tips. The rounded shape of the lobes was prefered over the conventional designs (that uses straight walls) for different reasons: the machining of the rounded shape is in consonance with the cooling and assembly approaches selected and it was been proved succesful by fabricating different models in copper and aluminum[14]. As the frequency profile was quite flat, we considered that it will not be necessary to change the cross section area (or the local volume of the cavity) to adapt to frequency changes. The cross section is then uniform for all the length of the RFQ.

The optimization of the geometry was made by running parametric simulations and selecting the optimum values with respect to minimizing power losses (or maximizing quality factor, Q_0). Mechanical constraints like the width of copper blocks, cooling channels diameter and corresponding wall thickness restricted the parametric optimization where one parameter was let free to match the frequency. The design frequency for the 2D models was chosen to be 348.6 MHz (several MHz below operating frequency) to avoid problems due to machining. The average modulation aperture of 3.438 mm was used as vane tip position. A sketch of the cross-section is shown in Fig. 9, while in 10 electric field lines for whole cross section in the quadrupole mode are shown.

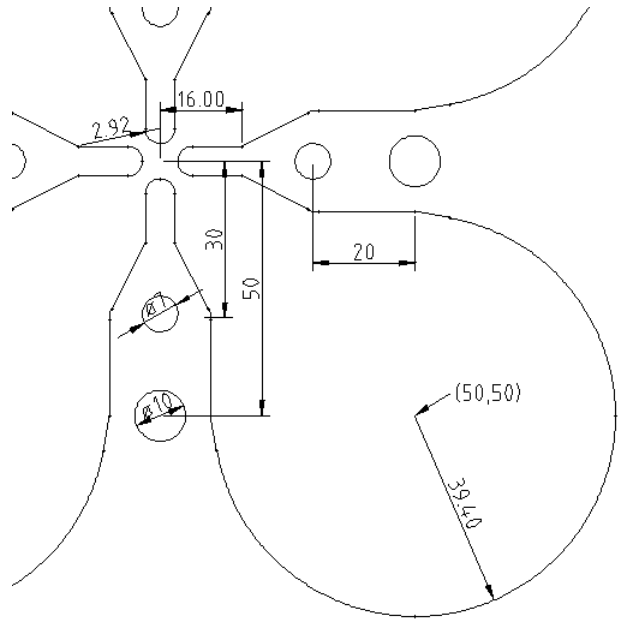

FIG. 9. Sketch of a portion of the RFQ cross section, showing some dimensions (all in mm). The vane tips geometry comes from the average values of the modulation and the cooling channels position and diameter, that restrict vane thickness due to impose a minimum wall thickness, are fixed values. All the other parameters were subject of optimization.

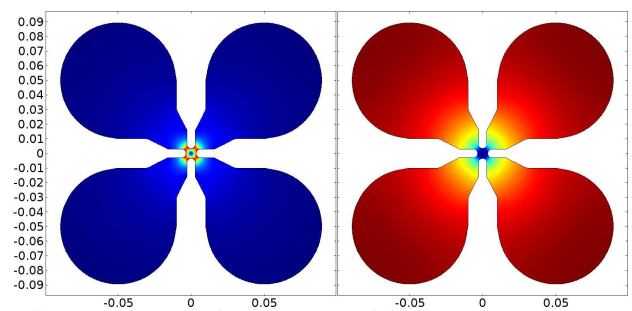

FIG. 10. Cross section of the RFQ, showing normalized electric (left) and magnetic (right) field distribution for the quadrupolar mode.

B. 3D cavity design

The 3D body of the cavity is constructed by extruding the cross-section, adding the vane modulation solids, the input and output regions and other details like tuner and vacuum ports. Again, the shape has been optimized by finite element simulations aiming at reducing power deposition. An overall longitudinal cross section is shown in fig. 11. The whole structure is an assembly of the four segments. Each segment has its own set of channels for cooling of the vanes and for cooling of the vacuum grid region.

The input and output undercut sections were designed so they have the same frequency as the bulk of the RFQ,

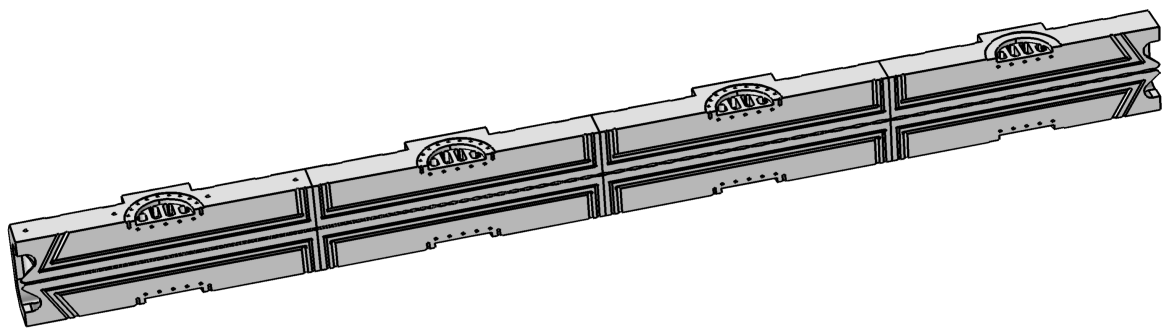

FIG. 11. Longitudinal cross section of the RFQ structure. The four segments can be seen, showing the cooling channels and the vacuum ports.

TABLE III. Parameters for input and output sections of the RFQ. Refer to Fig. 12 for description of parameters.

Parameter	**Input section**	**Output section**
R_{matcher} [mm]	16.674	14.0
z_{cover} [mm]	7.5	7.5
xy_{lobe} [mm]	88	88
r_{matcher} [mm]	25	25
z_{matcher} [mm]	22.60	21.0

contributing in this way to maintain the field flatness. The optimization was done in several geometry parameters, leaving one free in the optimization runs in order to match the desired frequency. Optimization was driven to reduce power losses in the section. A schematics of the input section with the optimization parameters is shown in fig. 12. Parameter values can be found in Table III.

The local frequency of the undercut resonators should be the same as the frequency of the bulk of the rest of the cavity. This frequency is controlled during design by changing the parameters shown in fig. 12. The distance between the end of the vane tip and the external input cover is let fixed at 7.5 mm. In the case that the fabricated cavity differs from the designed one, this local frequency can be corrected by changing the lid leaving more or less distance, thus changing the capacitive component of the frequency and adjusting it. This is a simpler operation than changing the cavity body.

The vacuum port grid changes slightly the local frequency of the cavity due to the openings it has. In order to compensate this detuning, the solid part of the grid penetrates the cavity as ridges, that have been also designed to provide the right frequency. These ridges are cooled by the vacuum port cooling channels. In the fabricated segments, they have been also rounded as the machining tool couldn't create sharp corners.

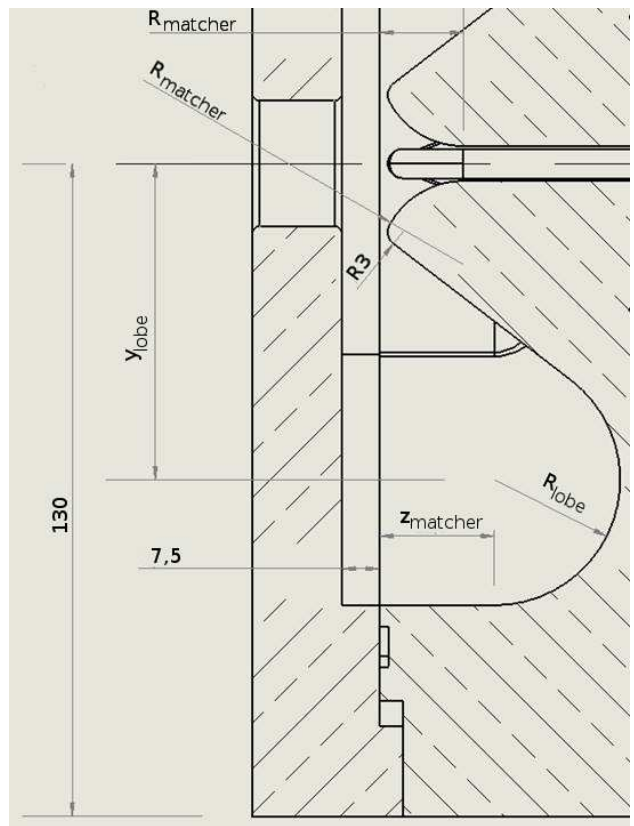

FIG. 12. Schematics of the input undercut section of the RFQ, showing the parameters chosen for optimization.

IV. ELECTROMAGNETIC SIMULATIONS AND TUNING

Electromagnetic FEM simulations of the whole length of the RFQ including the details of the modulation and undercuts require a lot of resources in preparation of the models and computation time. For this purpose, models with a simplified geometry are used. These models represent 1/8 of the RFQ volume, so effects that are out of this simmetry (like the vacuum ports) cannot be studied this way. These simulations are solved efficiently using COMSOL Multiphysics eigenvalue solver. A more detailed description was described elsewhere [15].

The central vane region must be defined very finely in order to catch all the details of the modulation. The description of the modulation must be done with accuracies of the order of tens of microns. The geometric construction of the vanes themselves is challenging, and we couldn't do it in a reliable way with COMSOL geometric modeler or using the CAD packages that we had available. A home made software that makes use of OpenCascade 3D technology[16] was coded and used for this.

The electrostatics (ES) simulations with constant voltage boundary condition, used during design of the RFQ modulation, are an approximation to the real RFQ cavity electromagnetic behaviour obtained by radiofrequency (EM) simulations. The intervane voltage in the resonator will not be uniform along its length due to local changes in frequency caused by the modulation itself and other perturbations. To study these effects a mathematical, transmission line model of the RFQ is needed[10]. Nevertheless, the ES simulations provide a way of scaling the values of the EM eigenfrequency simulations, as described below.

The values of electric and magnetic fields obtained from an eigenfrequency solution does not have the right amplitude that a real cavity during operation or testing will have: apart from the frequencies, only the spatial distribution of $\boldsymbol{E}$ and $\boldsymbol{B}$ is obtained. This is due to the fact that these models do not have an input power reference. To scale the fields, an scaling factor is obtained by comparing the electric field energy in the intervane region between ES and EM models. In the electrostatics model the vane voltage $\pm V_0/2$ is imposed as a boundary condition, so the magnitude of the electric field and the energy are known. The fields computed in the EM models will be multiplied by this factor to get the right scaling. This procedure is not exact, because distribution of electric field will be different in the both models. Although an iterative process has then be used to finally obtain the correct fields, we found that using volume averages the results obtained are satisfactory, as they compare very well with the results of the transmission line model (section IV B).

Another aspect to consider is how to compute the intervane voltage in the EM simulations, the following procedure was carried out:

For each $z = z_0$ a cross section of the intervane region is selected and electric field is extracted from it. The density of electric field energy is computed in the cross section surface Ω for the ES and scaled EM models:

$$W_{es} = \frac{1}{2}\int_{\Omega} \epsilon_0 E_{es}^2 d\Omega$$
$$W_{em} = \frac{1}{2}\int_{\Omega} \epsilon_0 (\alpha \cdot E_{em})^2 d\Omega \qquad (2)$$

where α is the scale factor. The energy in the electrostatic model will be also equal to $W_{es} = \frac{1}{2}C_l V_0^2$, where C_l is a capacitance per unit length. The capacitance only depends on geometrical considerations, so it must be the same in the ES and EM situation. So we can write

$$W_{em} = \frac{1}{2}C_l V(z)^2 \qquad (3)$$

and combining both:

$$V(z)^2 = \frac{W_{em}}{W_{es}} V_0^2 \qquad (4)$$

The voltage obtained this way is the same than the one that is described in a mathematical transmission-line model, and the one that must flat in the perfectly tuned RFQ. The capacitance per unit length $C_l(z)$ is obtained also as a result of this procedure. Again, this procedure is validated by the successful comparison of the results to the transmission line model (section IV B).

A. Static tuning

Static tuning of the RFQ is to be provided by a set of plunger tuners. For each segment of 800 mm there are 4 sets of 4 tuner ports, so a maximum of 64 tuners could be installed in the whole length (two ports will be used by the power couplers). The static tuners will increase the cavity frequency from the 348.6 MHz of the design to a value close to the operational frequency of 352.21 MHz. The voltage profile (field flatness) should be kept as uniform as possible during the process, and this will require that the tuners penetrate the cavity in a non-uniform way. This is studied with the transmission line model, but in the end will be verified experimentally.

B. Transmission line model

A transmission line model was developed to quickly analize the electromagnetic behaviour of the RFQ. In such a model[10] the intervane voltage and the frequency of the cavity are obtained using a perturbative approach. For the fundamental accelerating mode ($n = 0$) the model predicts a voltage described by

$$^{(1)}V_0(z) =^{(0)} V_0(z) + \sum_{m>0} a_{m0}\sqrt{\frac{2}{l_V}}\cos(k_m z) \qquad (5)$$

where

$$a_{m0} = -\sqrt{2}\frac{l_V}{(m\pi c)^2}\int_0^{l_V} \Delta\omega_0^2(z)\,\cos(k_m z)dz \qquad (6)$$

while the cavity frequency spectrum is obtained as

$$^{(1)}\omega_n^2 = ^{(0)}\omega_n^2 + \frac{2}{l_V}\int_0^{l_V} \Delta\omega_0^2(z)\cos^2(k_n z)dz \qquad (7)$$

In above equations the superindex (1) refers to the first order of perturbation, l_V is the vane length and $k_n = n\pi/l_v$ is the wave number. $\Delta\omega_0(z)$ is the change in local frequency with respect to the unperturbed, 2D frequency ω_0. In the case of the perturbation caused by the modulation, this function is directly the local frequency $\omega(z)$ discussed in section II D, so it is readily available. The perturbation caused by each of the plunger tuners and the undercuts are approximated using a Dirac δ function centered at the tuner position, and at $z = 0$ or $z = l_V$ respectively.

A comparison between the intervane voltage computed with the transmission line model and the voltage extracted computed from the FEM models of the whole length of the RFQ (following the procedure described in section IV), is shown in Fig. 13. The results obtained by both methods in all the circumstances that we considered compare very good. This, on one hand, validates the approach of scaling fields and voltage calculation described in the above sections and, on the other hand, validates the transmission-line model as a fine tool to study different tuning schemes. The FEM models take several hours (or days) to be prepared and computed, even with the automated framework developed by us, while a single run of the transmission-line model ends in a few seconds. An optimized voltage profile calculated this way and compared to the equivalent FEM model result is shown in Fig. 14. The transmission-line model is implemented in a Python program with a GUI to easily prepare and run calculations.

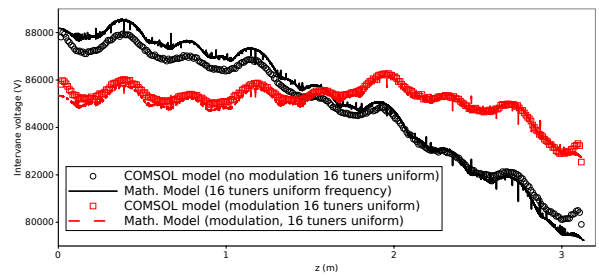

FIG. 13. Comparison of the intervane voltage computed using the transmission-line model (full lines) and the voltages extracted from the FEM model of the whole length of the RFQ (open markers). In one situation the vane modulation is not considered and in the other the full details are included. The overlapping of the FEM and the mathematical model curves is very good.

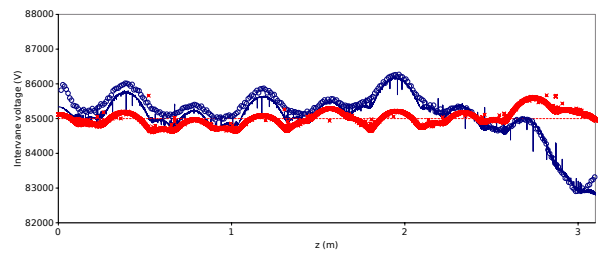

FIG. 14. An optimized voltage profile (in red) as compared to the original one without optimization (black).

V. COOLING DESIGN AND DYNAMIC TUNING

The RFQ is water cooled. The cooling removes the excess heat and also is used to fine tune the RFQ cavity during operation by controlling the thermal expansion driven frequency changes. For each segment, there are cooling channels near the vanes and also in the vacuum grid area.

A. Heat load

The heat load coming from the RF standing wave excited to the RFQ cavity walls is computed from the electromagnetic fields at the surface [10, 15]. The eigenfrequency problem is solved and the fields scaled as previously described. Power loss in the walls is computed with the expression (obtained using Poynting theorem in the cavity) as:

$$P = \frac{1}{2}R_s\int_S (\alpha H)^2 dS. \qquad (8)$$

where H is the magnetic field in the surface (always parallel to the surface) and R_s is the surface resistance, that is $R_s = \frac{1}{\sigma\delta_s}$, where σ is the electrical conductivity and $\delta_s = \sqrt{\frac{2}{\sigma\mu_0\omega}}$ the skin depth penetration. For copper at 352.2 MHz, with high surface roughness, the value used in the simulations is $R_s = 0.0052\,\Omega$. The factor α is the scale factor for the fields. The values obtained this way are the same as the ones obtained using a simulated input power coupler and impedance boundary conditions in the surface. Finally, power losses are multiplied by the duty factor, that ranges from 0 to 1, to calculate the average power lost in the walls per second. Estimations for the total power loss (at 5 % duty cycle) are shown in Table IV for different cases.

B. Water flow considerations

For the vane cooling channels the water inlets are located at the front of the segment and the outlets in the

TABLE IV. Power losses deposited in the RFQ surface, at duty cycle of 5%, for different conditions.

Model	f_{quad}	Losses (with covers)	Q_0
No tuners	349.3 MHz	17 508 W	10700
With tuners	352.2 MHz	17 158 W	10300

TABLE V. Flow average characteristics in the cooling channels. Channels type 1 and 2 are the vane cooling channels (type 1 are the exterior ones); channels type 3 are the vacumm grid cooling channels. The half in the input mass rate is due to having half a channel in the symmetric model computed. Magnitude shown are channel diameter, input mass rate, average velocity, kinematic viscosity and Reynolds number.

Type	⌀ (m)	Input (kg/s)	U (m/s)	$\nu, \frac{m^2}{s}$	Re
1	0.008	0.5*0.055	0.92	8.5×10^{-7}	8650
2	0.011	0.5*0.1	0.77	8.7×10^{-7}	9735
3	0.008	0.1	0.45	8.9×10^{-7}	4045

back, although these positions can be changed. Characteristics of the CFD simulations used in the thermo-mechanical calculations are shown in Table V. Thermo-mechanical simulations are done using a coupled CFD-thermo-mechanical approach, using a $k-\epsilon$ model for the turbulence modeling. The flow can be considered a fully developed turbulent flow, except in the acute pipe bending in the input matcher region of the vane modulation.

C. Thermo-mechanical results

Thermo-mechanical simulations are done using a model with a simplified geometry, without many of the external details of the RFQ structure. Simplification is made in order to increase the speed, particularly for transient simulations. The multiphysics framework of the simulations compute the electromagnetic fields from the RF eigenfrequency problem, uses the fields to compute the power input for the heat-transfer model, solves the coupled thermo-mechanical-CFD problem and from the mechanical deformation of the copper cavity finally computes the deformed volume of the vacuum region to recompute the resonant frequency from a new eigenfrequency calculation. In this way, the detuning caused by the thermo-mechanical deformations can be studied in any condition: steady state or transient simulations, with different RF duty cycles as power inputs and different water input temperatures and flows.

An example of the temperature distribution in the solid and the mechanical deformation can be seen in Fig. 15. For a duty cycle of the 5 % and the temperature of the input water fixed at 25 °C, the temperature of the copper is below 37 °C. In Fig. 16 the dependence of cavity frequency (first segment) with cooling water temperature is shown for steady state simulations.

Transient conditions have also studied this way, in order to use the cooling water temperature as a fine control during operation of the cavity frequency (thermal tuning). As an example of these calculations, in Fig. 17 the dynamic change of frequency during a power on step (and the opposite power off step) is shown. These results are used to tune a control model of the cavity frequency.

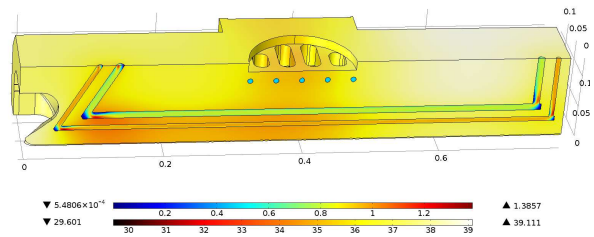

FIG. 15. Temperature distribution in the solid and water velocity in the cooling channels, obtained from the thermo-mechanical model of the first segment. Input power corresponds to a duty cycle of 5%. Water enters all the channels at 25 °C.

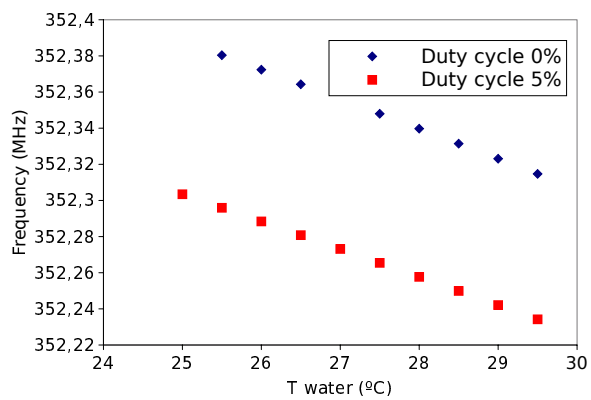

FIG. 16. Change in cavity frequency with cooling water temperature, for two different RF power conditions. The results come from steady-state simulations.

VI. FABRICATION

The fabrication of the first segment of ESS-Bilbao RFQ started in 2016. As mentioned before, Tye RFQ is a 4-vane structure. It has a total length of about 3.1 meters, divided in 4 segments of about 800 mm length each. The segment length is determined by the machining equipment available for fabrication of the vanes. Each segments is an assembly of four elements, 2 major and 2 minor vanes, assembled together by using polymeric vacuum gaskets instead of brazing or other welding system. Material is copper OHFC (Cu 10100) quality.

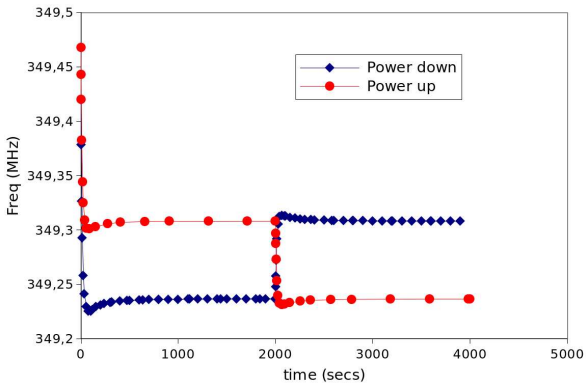

FIG. 17. Frequency of the RFQ cavity (first segment) during two different transient steps, from zero RF power to operation power at duty cycle 5 % (step power up) and the equivalent power down. Cavity frequency is computed at all times of the simulation.

A. Mechanical model

Starting from the electromagnetic design of the RFQ cavity a CAD model of the structure was built. The ports for tuners, vacuum grid and all other mechanical features were implemented in the model. RF and thermo-mechanical simulations were then ran again to validate the design.

The curve defining the modulation is defined in geometry construction by means of an interpolation of individual points. The transverse cross-section of the vane tip (semi-circular) is then extruded along the line of the modulation. The constructed geometry was then inspected to validate the geometry constructed: the curve corresponding to the modulation was extracted from the solids by different methods (directly from the STEP file format or after importing in COMSOL). We were not satisfied with the results obtained when comparing the extracted curves to the theoretical ones. We detected that discrepancies were caused by the construction of the initial curve done by the CAD software: the vane geometry is built from the extrusion along the curved line of the modulation of the semi-circular vane tip cross-section; this curve is itself built from the interpolation of the modulation description as a set of 3D points (200 points per modulation cell), but our CAD software did not perform correctly this interpolation. The result was a modulation curve with strong deviations from the design one.

A custom home-made code was then built, making use of OpenCascade kernel[16], to avoid this problem and build the modulation solids with great accuracy and control. This software can also create models of the RFQ vanes that were easy to mesh and to incorporate in FEM simulation procedures.

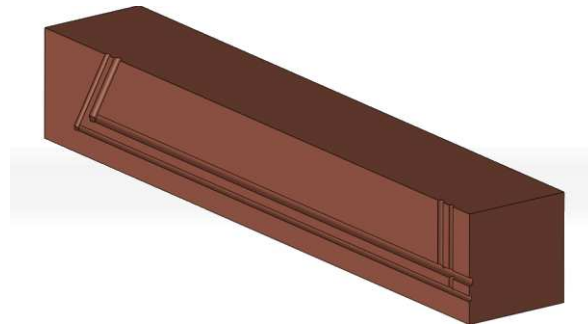

FIG. 18. Model showing the deep drilling of the longitudinal cooling channels.

B. Fabrication steps

1. *Raw material*

The material for the fabrication of the RFQ was supplied in blocks of two different sizes: 270x140 mm for major vanes and 115x140 mm for the minor ones. Length of all blocks is 830 mm. The copper grade selected is Cu OFE C10100.

2. *Squaring and deep drilling*

The first step in the fabrication process is to evenly square the copper blocks, to assure that each face is parallel to the opposing one and perpendicular to the others. Marks to fix the position of the cooling channels are machined in the corresponding faces.

A first rough machining is done, leaving an excess of about 2 mm, followed by a stress-relieve annealing. The deep drilling of the longitudinal cooling channels is then done. This is made during the first steps of the fabrication process, and channels will then serve as reference for the rest of the geometry. In this way, the effects of a possible deformation due to the machining is minimized as major machining is done afterwards. A model showing the channels is shown in Fig. 18. Fig. 19 shows a detail of the first fabricated vane after this stage.

At this stage, the two channels are connected and open in the back side (higher energy) of the RFQ segment. They will be sealed in a later step.

3. *EBW of the cooling channels plugs*

Cooling channels are then sealed by inserting copper plugs and welding them. This is carried out by our staff at ESS-Bilbaos Advanced Welding Facility by means of electron beam welding (EBW). Three plugs are inserted and welded, one to separate the two channels and the other two to seal them from the external face (Fig. 20). In the final steps of the process this face will be machined

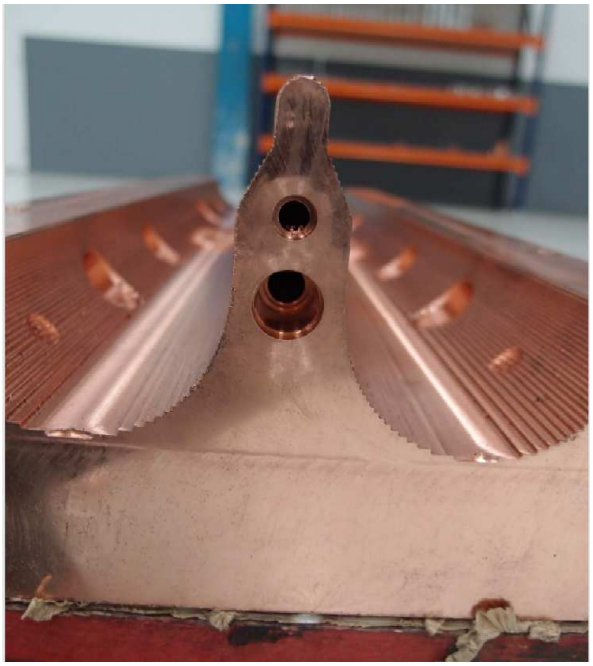

FIG. 19. A major vane after rough machining. The holes of the cooling channels can be seen in the vane.

and no external evidence of the welding of the plugs will be visible.

4. *Fine machining*

The last fabrication step for a vane is the fine machining, where all the final details are included. Particularly, the vane modulation needs a careful process in a temperature controlled machine to avoid over-heating that could give rise to deformations. Fig. 21 shows a major vane in the milling machine.

The milling of the modulation is made using a CAM controlled, 3-axes, HERMLE C800V machining centre. Many displacements of the tool on the copper surface are used, removing a very thin layer each step. This increases milling time but also provide excellent surface quality (roughness 0.8 Ra and mechanical tolerances around 0.005 mm.

5. *Metrology*

The final step is the metrology of the fabricated piece (Fig. 22). Special care is taken in the measurement of the vane modulation profile. After control of the first major vane, a deviation of the modulation measured with respect to the design one was detected, despite the attention paid to the machining process. To correct this, a second machining of the modulation profile was performed, lowering the height from the bottom face by 100 um.

FIG. 20. A major vane after cooling channels plugs have been inserted and welded by EBW.

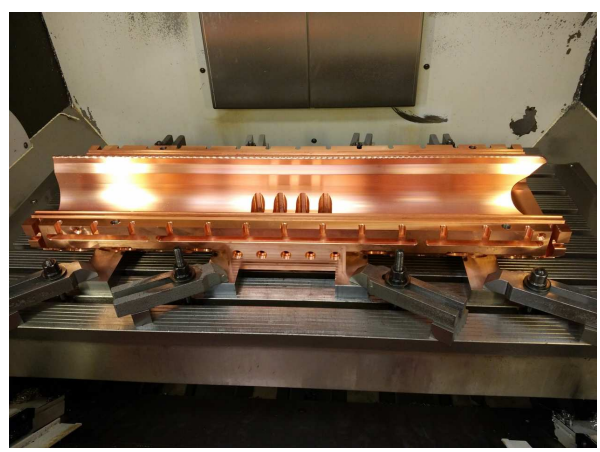

FIG. 21. A major vane of the RFQ after fine machining in the milling machine.

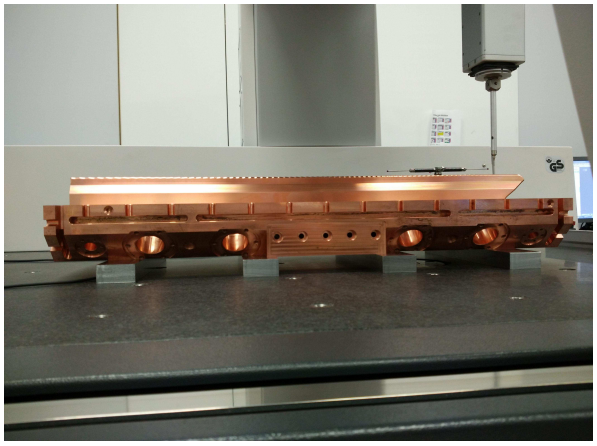

FIG. 22. Major vane in the metrology station.

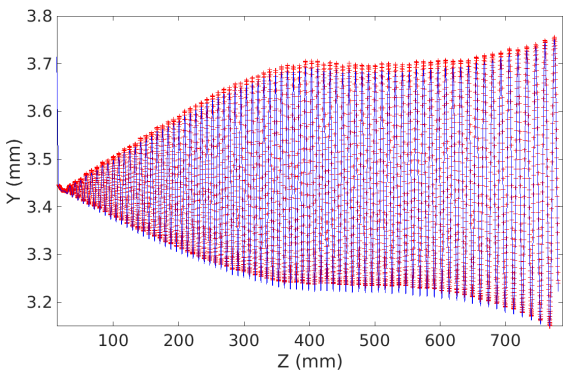

FIG. 23. Comparison of measured modulation to theoretical one.

The contact faces between major vanes and the two minor vanes were also machined removing the same height of material, so the four vane tips have the correct distribution after assembly.

Apart from this issue, the metrology results of the first vane of the first segment is very satisfactory (Fig. 23).

C. Assembly and vacuum strategy

The vacuum strategy for the cavity is based on the use of polymeric vacuum gaskets at the unions between major-minor vanes, and also on the contact faces between the assembly of four vanes and the cover or inter-segment ring. Once the four vanes are assembled (as in Fig. 1) and the alignment verified, the groove for the O-ring in the front side will be machined. This approach will allow assembling or disassembling the RFQ in case of misalignment or other problems. This strategy will be thoroughly tested with the first segment, in terms of vacuum levels and other issues. If results are satisfactory, the same procedure will be used for the rest of the segments. If results are negative, the strategy will be revisited and brazing of vanes will be considered. These results were planned to be presented in the contribution to IPAC 2017, but due to the several months delay on the fabrication tests have not yet been started.

VII. CONCLUSIONS

ESS-Bilbao RFQ design has been summarized, including details on the beam dynamics, cavity electromagnetic design, cooling and thermo-mechanical studies. Fabrication of the first segment of the RFQ is ongoing. The whole segment is expected to be received before the end of 2017 and vacuum and RF tests will then get started.

[1] ESS-Bilbao, "ESS-Bilbao," (2017).
[2] ESS, "European Spallation Source ERIC," (2017).
[3] Z. Izaola, I. Bustinduy, J. Corres, D. de Cos, C. de la Cruz, G. Harper, R. Miracoli, J. Muñoz, I. Rueda, A. Vizcaino, and A. Zugazaga, in *Proceedings of HB2016* (Malmo, Sweden, 2016) TUPMLY01.
[4] A. Letchford *et al.*, in *Proceedings of IPAC 2015* (Richmond, VA, USA, 2015) THPF105.
[5] C. Rossi *et al.*, in *Proceedings of LINAC'08* (Victoria, BC, Canada, 2008) MOP040.
[6] I. Bustinduy and J. L. Muñoz, eds., *Technical Design Report: ESS-Bilbao RFQ* (2015).
[7] J. Staples, S. Abbott, R. Caylor, R. Gough, D. Howard, and R. MacGill, in *Proceedings of 1988 Linear Accelerator Conference* (Williamsburg, Virginia, USA, 1988).
[8] I. M. Kapchinsky and V. A. Tepliakov, *A Linear Ion Accelerator with Spatially Uniform Hard Focusing*, Tech. Rep. (Stanford Linear Accelerator Center, 1969) sLAC-TRANS-0099.
[9] A. Letchford and A. Schempp, in *Proceedings of EPAC 98 Conference* (Stockholm, Sweden, 1998).
[10] T. Wangler, *RF Linear Accelerators*, Physics textbook (Wiley, 2008).
[11] M. J. Browman and L. Young, in *Proceedings of LINAC1990* (Albuquerque, USA, 1990) p. 70, a-12004-C.
[12] *General Particle Tracer User Manual (v. 2.82)*, Pulsar Physics.
[13] R. Duperrier, *Intense beam dynamics in RFQs linacs*, Ph.D. thesis, University of Orsay, Orsay (2000).
[14] I. Bustinduy and J. M. et al., in *Proceedings of IPAC 2012, THEPPB001* (New Orleans, Luisiana, USA, 2012).
[15] J. Muñoz, D. de Cos, I. Madariaga, and I. Bustinduy, in *Proceedings of COMSOL Conference 2015* (2015).
[16] Open Cascade, "Open Cascade Technology," (2017).